

Parameters affecting the determination of transport kinetics data in highly swelling polymers above T_g

M.S. Hedenqvist, U.W. Gedde*

Royal Institute of Technology, Department of Polymer Technology, S-100 44 Stockholm, Sweden
 Packforsk-Swedish Packaging Research Institute, Box 9, S-164 93 Kista, Sweden

Received 2 April 1998; accepted 2 June 1998

Abstract

Sorption and desorption data for n-hexane–natural rubber and n-hexane–low-density polyethylene were analysed to reveal the cause of the s-shaped sorption curves frequently occurring in highly swollen polymers. The model permitted the influence of solute-concentration-dependent diffusivity, sample geometry, boundary concentrations and swelling-induced mechanical stresses on the transport data to be examined. The calculated solute diffusivity varied by several orders of magnitude, depending on the choice of parameters included in the model. The inclusion of direct mechanical stress relaxation parameters only gave a slight improvement of the fit to the experimental data. The inclusion of a time-dependent surface concentration was the only way to fit the s-shaped sorption curves for both natural rubber and low-density polyethylene. Although isotropic three-dimensional swelling of natural rubber occurred over the whole sorption transient period, this condition was unable to explain the swelling (thickness increase) of low-density polyethylene. In the latter system, a model consisting of two stages had to be adopted: stage I where the swelling was mainly one-dimensional, and stage II which occurred later and was characterized by three-dimensional swelling similar to that occurring in natural rubber. During the transient sorption period, the ratio between natural rubber and low-density polyethylene of the ratio of the thickness to cross-sectional area was close to their bulk modulus ratio, which suggests that it is the bulk modulus rather than the Young's modulus which determines the sorption characteristics of polymers above T_g . © 1999 Elsevier Science Ltd. All rights reserved.

Keywords: S-shaped sorption curves; Highly swollen polymers; Transport kinetics

1. Nomenclature

| | | | |
|-----------------|--|--------------------|---|
| μ_1^0 | chemical potential at a solute activity equal to unity | a_1 | activity of penetrant |
| μ_1 | solute chemical potential | A_i | cross-sectional area at x_i |
| α_{De} | constant describing the magnitude of concentration dependence of D in Eq. (4) | α_K | constant describing the magnitude of concentration dependence on K |
| α_{DI} | constant describing the magnitude of concentration dependence of D in Eq. (5) | α_{τ_m} | constant describing the magnitude of concentration dependence on τ_m |
| σ_{xx}^s | solute-induced mechanical stress at equilibrium solute concentration in the x -direction | α_{τ_s} | constant describing the magnitude of concentration dependence on τ_s |
| σ_{xx} | solute-induced mechanical stress in the x -direction | C, C_1 | solute concentration |
| \bar{V}_1 | solute molar volume | D | diffusion coefficient |
| D_{coe} | zero concentration diffusivity in Eq. (4) | $D_{a,b}$ | diffusion coefficient for layer a and b |
| D_{col} | zero concentration diffusivity in Eq. (5) | D_{co} | diffusion coefficient at zero solute concentration |
| | | err | integration error in the Runge–Kutta method |
| | | ε_{xx} | strain in the x -direction |
| | | F_o | rate of evaporation |
| | | h | step length in the spatial direction |
| | | i | integer number of the spatial position |
| | | j | integer number of the time position |
| | | K | bulk modulus |
| | | k_1, k_2, k_3 | constants in the Runge–Kutta method |
| | | K_{co} | bulk modulus at zero solute concentration |

* Corresponding author.

| | |
|--------------------------|---|
| l | plate thickness |
| L | thickness of half the plate |
| $M_{i,t}$ | mass uptake or loss in element i at time t |
| $M_t^{(\infty)}$ | equilibrium solute mass uptake per original sample cross-sectional area |
| n | number of x -coordinates |
| P | hydrostatic pressure |
| R | the gas constant |
| ρ_1 | solute density |
| ρ_2 | polymer density |
| σ | solute-induced mechanical stress |
| sp | constant describing three dimensional swelling |
| T | temperature |
| t | time |
| τ_{mco} | stress relaxation time at zero solute concentration |
| tol | absolute tolerance for the Runge–Kutta integration |
| tol1 | relative tolerance for the Runge–Kutta integration |
| τ_{sco} | surface concentration relaxation time at zero solute concentration |
| u | thickness of solute-free sample |
| $V_{i,t}$ | volume of element i at time t |
| $w_{1,2}$ | mass fractions of solute (1) and polymer (2) respectively |
| x | space coordinate |
| ξ | partition coefficient |
| $\Delta(2L)_{\text{nd}}$ | normalized thickness decrease |
| $\Delta(2L)_{\text{ni}}$ | normalized thickness increase |
| ΔA_{nd} | normalized cross-sectional decrease |
| ΔA_{ni} | normalized cross-sectional increase |
| Δm_{nd} | normalized mass decrease |
| Δm_{ni} | normalized mass increase |
| ΔV_{nd} | normalized volume decrease |
| ΔV_{ni} | normalized volume increase |

2. Introduction

A sorption–desorption experiment is an easy way of obtaining transport kinetics data for gases, vapours and liquids in polymers [1]. The number of parameters that can be determined from the sorption–desorption technique is greater than from the permeability techniques available, and for liquid solutes the sorption–desorption technique is outstanding [2].

In many polymer–solute systems, the calculation of transport properties from sorption–desorption experiments is, however, difficult due to interactions between the matrix and the penetrating molecules. Despite the complexity, simplified calculations of the diffusion coefficient (D) are performed which in the worst cases can lead to deviations from the ‘true’ value of D by several orders of magnitude. It is thus very important that the calculation of D from sorption–desorption experiments includes all the factors that affect the sorption–desorption behaviour. Crank [3], Comyn [4], Crank and Park [5] and Neogi [6] present reviews of the different anomalous phenomena that may occur during sorption and desorption.

The most frequently occurring ‘anomaly’ connected with sorption is probably the sigmoidal- (s-) shape of the sorption curve which is observed when the amount of solute absorbed is plotted as a function of the square root of time. It occurs in systems where the solute is absorbed in high concentrations in the polymer, regardless of whether the polymer is glassy, rubbery, amorphous or semicrystalline, and regardless of whether a phase transition accompanies the solute uptake [7]–[13]. Suggestions regarding the origin of the s-shape include stress-effects [7], [9], [11], [13]–[15] simple swelling [10], [16], coupled diffusion and thermal effects [17], a surface layer with different properties than those of the interior [18] and solvent-induced plasticization of the polymer [8].

The most widely used method of modelling s-shaped sorption curves is to include a time-dependent surface boundary concentration in the model [2], [13], [19]–[21]. This time-dependence is considered to be due to the fact that, during the transient sorption period, the swollen surface is subjected to compressive stresses caused by the unswollen interior of the sample. This approach fits sorption data well, but it may be a simplification because it only indirectly considers the concentration–stress relationships that exist in the sample during the transient swelling period. It is therefore important to determine whether a more detailed diffusion–stress model reveals any new aspects of the sorption–desorption phenomenon.

In this paper, several parameters are examined and their impact on the s-shaped sorption curve is analysed in detail to elucidate what parameters primarily affect the s-shape and what parameters should be included in a determination of transport properties from sorption data for highly swollen systems. These parameters include solute-concentration dependence of the diffusivity, swelling, variable boundary concentration and swelling-induced mechanical stresses. The systems examined are a loosely crosslinked natural rubber and a low-density polyethylene (LDPE), both immersed in n-hexane.

3. Experimental

The samples studied were a low-density polyethylene (LDPE, 1.5 mol% ethyl branches, $\overline{M}_w = 127\,000 \text{ g mol}^{-1}$, $(\overline{M}_w)/(\overline{M}_n) = 7.5$, mass crystallinity $w_c = 0.54$, $\rho_2 = 918 \text{ kg m}^{-3}$ (298.2 K)) and a crosslinked natural rubber (NR, $\overline{M}_w = 664\,000 \text{ g mol}^{-1}$, $(\overline{M}_w)/(\overline{M}_n) = 4.6$, $\rho_1 = 920 \text{ kg m}^{-3}$ (298.2 K)). $\overline{M}_c = 2500 \text{ g mol}^{-1}$ for the cross-linked NR from n-hexane sorption equilibrium data. Morphological data for the LDPE are presented in Ref. [22], sample B2. The LDPE was melt-crystallized during cooling at a rate of 15 K min^{-1} from 443 K in a Schwabenthan compression moulding machine (Polystat 400s).

The dimensions of the unswollen samples used in the sorption–desorption experiments were: LDPE — thickness = 1.938 mm , width = 100 mm , length = 100 mm ; NR —

2.715–3.46 mm × 32.6 mm × 32.6 mm. The samples were immersed in liquid n-hexane [purity 99%, Merck, density; $\rho_1 = 656 \text{ kg m}^{-3}$ (298.2 K)] at 298.2 K and intermittently weighed until sorption equilibrium was attained. Prior to each weighing, the samples were surface dried. Three hours after sorption equilibrium was established, the surface-dried samples were exposed to air at 298.2 K and the desorption was monitored by intermittent weighing of the samples on a Mettler AE balance after different times. The loss of polymer material into the n-hexane liquid during sorption was low [$< 2 \text{ wt\%}$ (NR) and $< 0.6 \text{ wt\%}$ (LDPE)].

The computer calculations were performed on a SUN Sparc Ultra 2 ($2 \times 200 \text{ MHz}$) workstation with codes written in Fortran F77.

4. Model scheme

4.1. Concentration dependence

Fick's second law of diffusion, which can be expressed as

$$\frac{\partial C_1}{\partial t} = \frac{\partial}{\partial x} \left(D(C_1) \frac{\partial C_1}{\partial x} \right) \quad (1)$$

was solved for a plate geometry (Fig. 1) where C_1 is the penetrant concentration (g cm^{-3}), x is the thickness coordinate and t is time. Only half of the plate thickness was considered, and the inner boundary coordinate was described as an isolated point:

$$\left(\frac{\partial C_1}{\partial x} \right)_{x=L} = 0 \quad (2)$$

and the outer boundary was kept constant in time during the sorption ($C_1 = C_1^{\text{eq}}$). During desorption, evaporation takes place at the surface:

$$D(C_1) \left[\frac{\partial C_1}{\partial x} \right]_{x=0} = F_o C_1 \quad (3)$$

where F_o is the evaporation constant determined to be between 5×10^{-6} and $5 \times 10^{-5} \text{ cm s}^{-1}$ for both materials

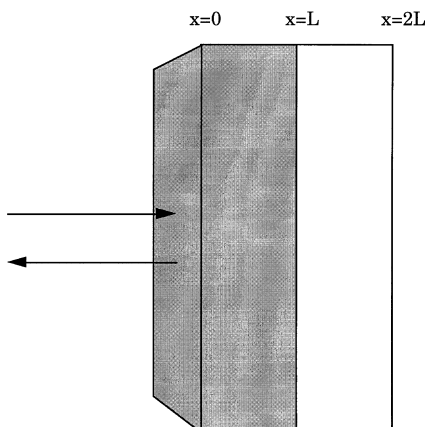


Fig. 1. Migration into and out of a plate using plate symmetry conditions.

using a procedure of Bakhouya et al. [23]. In the following treatment, the index 1 is left out for simplicity. Two different kinds of equations were used to describe the concentration-dependent diffusivity [$D(C)$]:

$$D(C) = D_{\text{coe}} e^{\alpha_{\text{De}} C} \quad (4)$$

$$D(C) = D_{\text{col}} (1 + \alpha_{\text{DI}} C) \quad (5)$$

where D_{coe} and D_{col} are zero concentration diffusivities and α_{De} and α_{DI} are constants depending on the type of polymer and solute.

Eq. (1), implementing Eq. (4), is discretized according to:

$$\frac{\partial C}{\partial t} = f(t, C) \\ = \frac{D_{\text{coe}}}{\Delta x_i^2} (e^{\alpha_{\text{De}} C_{i+0.5}} (C_{i+1} - C_i) - e^{\alpha_{\text{De}} C_{i-0.5}} (C_i - C_{i-1})) \quad (6)$$

where

$$C_{i\pm 0.5} = \frac{C_i + C_{i\pm 1}}{2} \quad (7)$$

Eq. (2) is best discretized using

$$C_{n+1} = C_{n-1} \quad (8)$$

($i = n$ at centre of plate), and the surface boundary condition [Eq. (3)] may be written explicitly, including Eq. (4), as ($i = 0$ at the boundary):

$$C_0 = \frac{C_1}{1 + \frac{\Delta x_i F_o}{D_{\text{coe}} e^{\alpha_{\text{De}} C_1}}} \quad (9)$$

The concentration profiles were generated using the following implicit multistep method (j is time coordinate):

$$\nabla^3 C_{j+1} = \frac{6}{11} \Delta t_j \left(f(t_{j+1}, \nabla^3 C_{j+1} + \nabla^2 C_j + \nabla C_j + C_j) \right. \\ \left. - \frac{1}{\Delta t_j} \left(\frac{3}{2} \nabla^2 C_j + \nabla C_j \right) \right) \quad (10)$$

The details of the method is described by Hedenqvist et al. [24]. The implicit method integrates with respect to time using arcs with three constant time steps, but with a variable step size between them. The first arc is produced by a three-stage second-order Runge–Kutta method [25]:

$$k_1 = f(t_j, C_j) \quad (11)$$

$$k_2 = f(t_j + \Delta t_j, C_j + \Delta t_j k_1) \quad (12)$$

$$k_3 = f(t_j + 0.5 \Delta t_j, C_j + 0.25 \Delta t_j [k_1 + k_2]) \quad (13)$$

If the error:

$$\text{err} = \Delta t_j \frac{k_1 - 2k_3 + k_2}{3} \quad (14)$$

is less than the tolerance:

$$\text{tol} = \text{tol1} \cdot \max(C_j, 1) \quad (15)$$

where tol1 is the relative tolerance kept at 0.001, the

solution is updated:

$$t_{j+1} = t_j + \Delta t_j \quad (16)$$

$$C_{j+1} = C_j + \Delta t_j \frac{k_1 + 4k_3 + k_2}{6} \quad (17)$$

Otherwise, a smaller step size is selected and the scheme (Eqs. (11)–(15)) is computed again. The new step size is determined according to:

$$\Delta t_{j+1} = \min \left(\Delta t_{\max}, 0.9 \Delta t \left[\frac{\text{tol}}{\text{err}} \right]^{\frac{1}{3}} \right) \quad (18)$$

where Δt_{\max} is the maximum step size allowed. The concentration profiles were integrated using Simpson's method with the Romberg routine to obtain higher accuracy.

4.2. Stress phenomena and change in plate dimension

The stress build-up in the plate during extensive swelling may lead to a time-dependent surface concentration [19], [21]. The concentration is therefore described by:

$$\left[\tau_s \frac{\partial C}{\partial t} \right]_{x=0} + (C - C_\infty)_{x=0} = 0 \quad (19)$$

where C_∞ is the final concentration calculated as:

$$C_\infty = \frac{w_1 \rho_2}{1 + \frac{w_1 \rho_2}{\rho_1}} \quad (20)$$

and τ_s is the surface concentration relaxation time which shows a solute concentration dependence through α_{τ_s} :

$$\tau_s = \tau_{\text{sc}} e^{-\alpha_{\tau_s} C} \quad (21)$$

and w_1 is the n-hexane equilibrium mass concentration: 1.3302 kg (kg NR)⁻¹ and 0.1103 kg (kg LDPE)⁻¹, both at 298.2 K. The initial boundary concentration is C_0 . During desorption, the surface concentration may be described by Eq. (9).

In a more detailed treatment, the stress effects have to be considered throughout the thickness of the plate coupled with the changes in sample dimensions following swelling. The bases of the following derivations originate from Bakhouya et al. [23] and Wu and Peppas [26]. The mass increase rate or mass loss rate in a swelling element (Fig. 2) is given by:

$$\frac{\partial M}{\partial t} = -AD \frac{\partial C}{\partial x} \quad (22)$$

where A is the cross-sectional area. This equation may also be expressed as:

$$\frac{\partial M}{\partial t} = -AD \frac{\partial C}{\partial \mu_1} \frac{\partial \mu_1}{\partial x} \quad (23)$$

The chemical potential (μ_1) is related to the penetrant

activity (a_1) and the swelling pressure (P) through:

$$\mu_1 = \mu_1^0 + RT \ln(a_1) + \bar{V}_1 P \quad (24)$$

where μ_1^0 is the chemical potential at the penetrant activity equal to unity and \bar{V}_1 is the molar volume of the penetrant which is $\bar{V}_1 = 131.1 \text{ cm}^3 \text{ mol}^{-1}$. The chemical potential gradient may be divided into two different terms:

$$\frac{\partial \mu_1}{\partial x} = \frac{\partial \mu_1}{\partial a_1} \frac{\partial a_1}{\partial C} \frac{\partial C}{\partial x} + \frac{\partial \mu_1}{\partial P} \frac{\partial P}{\partial x} \quad (25)$$

Neglecting inertial terms and shear stresses [27], [28] and considering only the x -direction yields:

$$\frac{\partial P}{\partial x} = \frac{\partial \sigma_{xx}}{\partial x} \quad (26)$$

where σ_{xx} is the x -dimensional normal stress defined as positive for a compressive stress. Combination of Eqs. (23)–(26) leads to:

$$\frac{\partial M}{\partial t} = -AD \left(\frac{\partial C}{\partial x} + \frac{\bar{V}_1 C}{RT} \frac{\partial \sigma_{xx}}{\partial x} \right) \quad (27)$$

The mass uptake rate or mass loss rate in element ' i ' may therefore, for simplicity, be expressed as the sum of a 'concentration'-term and a 'stress'-term:

$$\frac{\partial M_{i,t}}{\partial t} = \frac{\partial M_{i,t}^c}{\partial t} + \frac{\partial M_{i,t}^\sigma}{\partial t} \quad (28)$$

which may be further written (Fig. 2) as:

$$\frac{\partial M_{i,t}^c}{\partial t} = \left(AD \frac{\partial C}{\partial x} \right)_{i+0.5} - \left(AD \frac{\partial C}{\partial x} \right)_{i-0.5} - \Delta u \left(\frac{\partial A}{\partial u} D \frac{\partial C}{\partial x} \right)_i \quad (29)$$

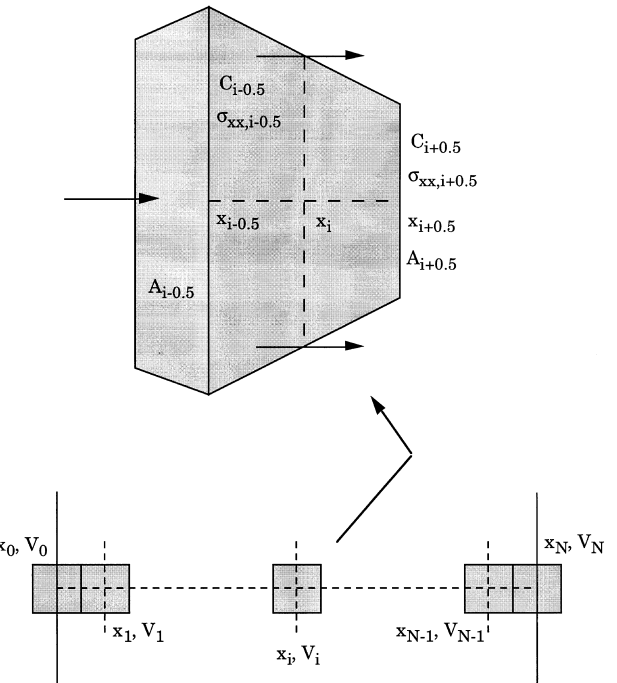


Fig. 2. Schematic representation of the swelling element with definitions of parameters.

and

$$\frac{\partial M_{i,t}^\sigma}{\partial t} = \left(AD \frac{\bar{V}_1 C}{RT} \frac{\partial \sigma_{xx}}{\partial x} \right)_{i+0.5} - \left(AD \frac{\bar{V}_1 C}{RT} \frac{\partial \sigma_{xx}}{\partial x} \right)_{i-0.5} - \Delta u \left(\frac{\partial A}{\partial u} D \frac{\bar{V}_1 C}{RT} \frac{\partial \sigma_{xx}}{\partial x} \right)_i \quad (30)$$

$$C_{i,t} = \frac{M_{i,t}}{\left(\Delta u + \frac{M_{i,t}}{\rho_1} \right)} \quad (31)$$

where Δu is the dry sample thickness and $M_{i,t}$, $M_{i,t}^c$, $M_{i,t}^\sigma$ are the mass contents per dry unit area of each element i . Eqs. (29) and (30) may be discretized according to Eqs. (32) and (33), assuming that the change in dimensions at each point is described by the constant sp [$sp = (1/3)$ when the change is equal in all directions and $sp = 1$ when swelling occurs only in the x -direction] and that the swelling or shrinkage is linear with respect to the coordinate x .

$$\begin{aligned} \frac{\partial M_{i,t}^c}{\partial t} = & \left[\left(1 - \frac{C_{i+0.5}}{\rho_1} \right)^{sp-1} D_{i+0.5} \frac{C_{i+1} - C_i}{x_{i+1} - x_i} \right] \\ & - \left[\left(1 - \frac{C_{i-0.5}}{\rho_1} \right)^{sp-1} D_{i-0.5} \frac{C_i - C_{i-1}}{x_i - x_{i-1}} \right] \\ & + \left[\left(\left(1 - \frac{C_{i-0.5}}{\rho_1} \right)^{sp-1} - \left(1 - \frac{C_{i+0.5}}{\rho_1} \right)^{sp-1} \right) \right. \\ & \times D_i \frac{C_{i+1} - C_{i-1}}{x_{i+1} - x_{i-1}} \left. \right] \quad (32) \end{aligned}$$

and

$$\begin{aligned} \frac{\partial M_{i,t}^\sigma}{\partial t} = & \frac{\bar{V}_1}{RT} \left[\left(1 - \frac{C_{i+0.5}}{\rho_1} \right)^{sp-1} D_{i+0.5} C_{i+0.5} \frac{\sigma_{xx,i+1} - \sigma_{xx,i}}{x_{i+1} - x_i} \right] \\ & - \frac{\bar{V}_1}{RT} \left[\left(1 - \frac{C_{i-0.5}}{\rho_1} \right)^{sp-1} D_{i-0.5} C_{i-0.5} \frac{\sigma_{xx,i} - \sigma_{xx,i-1}}{x_i - x_{i-1}} \right] \\ & + \frac{\bar{V}_1}{RT} \left[\left(\left(1 - \frac{C_{i-0.5}}{\rho_1} \right)^{sp-1} - \left(1 - \frac{C_{i+0.5}}{\rho_1} \right)^{sp-1} \right) \right. \\ & \times D_i C_i \frac{\sigma_{xx,i+1} - \sigma_{xx,i-1}}{x_{i+1} - x_{i-1}} \left. \right] \quad (33) \end{aligned}$$

where

$$C_{i\pm 0.5} = \frac{C_i \pm C_{i\pm 1}}{2} \quad (34)$$

and $D = D(C)$ is given by Eq. (4). The x -coordinates are calculated from

$$\begin{aligned} x_i = & \Delta u \left[0.5 \left(1 - \frac{C_0}{\rho_1} \right)^{-sp} + \sum_{i=1}^{i-1} \left(1 - \frac{C_i}{\rho_1} \right)^{-sp} \right. \\ & \left. + 0.5 \left(1 - \frac{C_{i-0.25}}{\rho_1} \right)^{-sp} \right] \quad (35) \end{aligned}$$

where

$$C_{i-0.25} = 0.25 C_{i-1} + 0.75 C_i \quad (36)$$

The stress–strain properties are described for simplicity by the Maxwell element:

$$\frac{\partial \sigma_{xx}}{\partial t} = K \frac{\partial \varepsilon_{xx}}{\partial t} - \frac{1}{\tau_m} (\sigma_{xx} - \sigma_{xx}^s) \quad (37)$$

The relaxation time (τ_m) and the bulk modulus (K) depend on the solute concentration according to:

$$\tau_m = \tau_{m0} e^{-\alpha_{\tau_m} C} \quad (38)$$

$$K = K_{c0} e^{-\alpha_K C} \quad (39)$$

where τ_{m0} and K_{c0} are the zero concentration relaxation time and zero concentration bulk modulus. α_{τ_m} and α_K are constants. Eq. (37) may be discretized according to:

$$\sigma_{xx,j+1} = \sigma_{xx,j} + K(\varepsilon_{xx,j+1} - \varepsilon_{xx,j}) - \frac{\Delta t}{\tau_m} (\sigma_{xx,j} - \sigma_{xx,j}^s) \quad (40)$$

or alternatively

$$\sigma_{xx,j+1} = \left(1 + \frac{\Delta t}{\tau_m} \right)^{-1} \left(\sigma_{xx,j} + K(\varepsilon_{xx,j+1} - \varepsilon_{xx,j}) + \frac{\Delta t}{\tau_m} \sigma_{xx,j}^s \right) \quad (41)$$

Assuming volume additivity, the strain in the x -direction is given by:

$$\varepsilon_{xx} = \left(1 - \frac{C}{\rho_1} \right)^{-sp} - 1 \quad (42)$$

The total mass uptake or mass loss (M_t) per unit dry area is calculated as:

$$M_t = 0.5 C_{0,t} V_{0,t} + \sum_{i=1}^{N-1} C_{i,t} V_{i,t} + 0.5 C_{N,t} V_{N,t} \quad (43)$$

where the volume of element i is:

$$V_{i,t} = \frac{\Delta u}{\left(1 - \frac{C_{i,t}}{\rho_1} \right)} \quad (44)$$

The total mass uptake or mass loss (M_t) is obtained as a function of time by integrating Eq. (28) using the previously described Runge–Kutta method. After the initial values of C_i , V_i , x_i , ε_i , $\sigma_{xx,i}$ are calculated the integration is performed in the following order: M_i [Eq. (28)] $\rightarrow C_i$ $\rightarrow V_i$ $\rightarrow x_i$ $\rightarrow \varepsilon_i$ $\rightarrow \sigma_i \rightarrow M_t$.

Eq. (43) yields the same result whether N is 60 or 40 and a value of 40 was, therefore, used to increase the integration speed. At the boundary elements ($x = 0$ and $x = x_N$):

$$\frac{\partial M_t}{\partial t} = 0 \quad (45)$$

and the concentration is calculated explicitly using Eq. (19). x_N is calculated using $C_{N-0.25} = C_N$ in Eq. (35).

4.3. Layer structure

In order to simulate penetrant transport in a 2-layer material (Fig. 3), Eq. (1) is solved using the multivalue method described earlier; only half the plate thickness is considered. In order to maintain mass balance between layers a and b, the following relationship describes the boundary condition:

$$D_a(C_a) \frac{\partial C_a}{\partial x_a} = D_b(C_b) \frac{\partial C_b}{\partial x_b} \quad (46)$$

A discretized approximation to Eq. (46) ($i = k$ at the boundary point, $i =$ space coordinate) is:

$$D_a(C_{a,k-0.5}) \frac{C_{a,k} - C_{a,k-1}}{x_k - x_{k-1}} = D_b(C_{b,k+0.5}) \frac{C_{b,k+1} - C_{b,k}}{x_{k+1} - x_k} \quad (47)$$

The partition coefficient (ξ) is defined as:

$$\xi = \frac{C_b^\infty}{C_a^\infty} \quad (48)$$

where C_a^∞ and C_b^∞ are the saturation concentrations of solute in layers a and b respectively. Eqs. (47) and (48) are combined to yield the boundary concentration:

$$C_{a,k} = \frac{C_{a,k-1} + \frac{D_b(\xi C_{a,k+0.5})}{D_a(C_{a,k-0.5})} \xi C_{a,k+1}}{1 + \frac{D_b(\xi C_{a,k+0.5})}{D_a(C_{a,k-0.5})} \xi} \quad (49)$$

where

$$C_{a,k\pm 0.5} \equiv C_{a,k\pm 0.5}^{(j)} = \frac{C_{a,k}^{(j-1)} + C_{a,k\pm 1}^{(j)}}{2} \quad (50)$$

The outer boundary concentration was held at $C = C_a^\infty$ during sorption and $C = 0$ during desorption, and the inner boundary was described by Eq. (2).

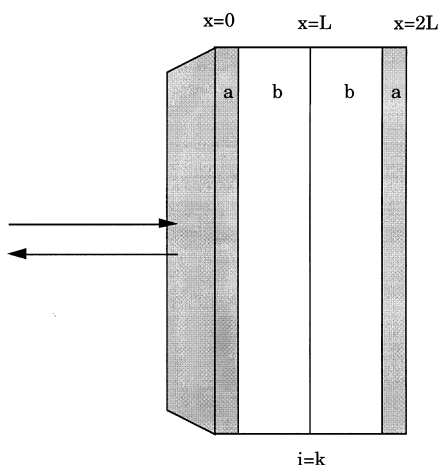


Fig. 3. Schematic diagram of the three-layer plate.

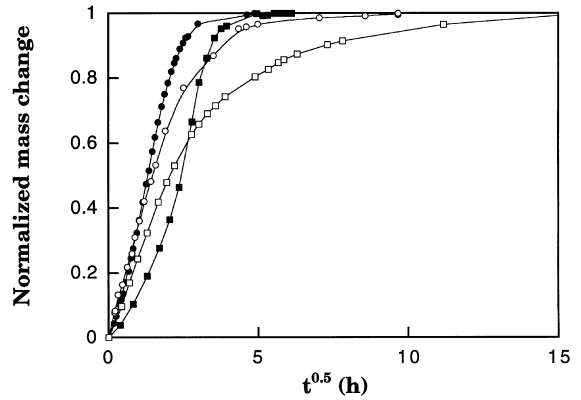


Fig. 4. n-Hexane sorption (●, NR; ■, LDPE) and desorption (○, NR; □, LDPE) curves.

5. Results and discussion

Since sorption and desorption curves intersect in Fig. 4, it is clear that the n-hexane diffusivities in both NR and LDPE are functions of solute concentration. In Fig. 5, Eqs. (4) and (5) are fitted to desorption-data in NR. Both the dry and the swollen sample thicknesses were used in the calculations. The choice of sample thickness affects only the zero-concentration diffusivity and does not alter the desorption curve shape. Both equations fit the desorption data well and it was also found that the desorption concentration profiles are essentially identical. The desorption concentration profiles using Eq. (5) are shown in Fig. 6. Eqs. (4) and (5) are frequently used to describe concentration-dependent diffusivities and it is difficult to select the most appropriate of these equations on the basis of curve fitting to the experimental data. A reason to prefer Eq. (4) over Eq. (5) is that the former is a semi-empirical relationship originating from concentration-viscosity behaviour[29].

To see whether the s-shaped sorption curve can be described by a high concentration dependence alone, the

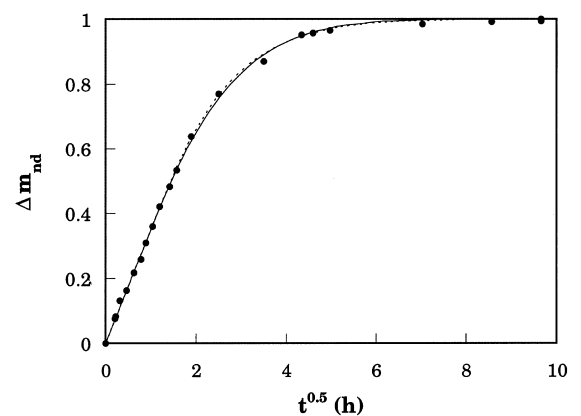


Fig. 5. Best fit to experimental (●) n-hexane desorption data in NR using exponential [Eq. (4), continuous line] and linear [Eq. (5), broken line] concentration dependence; $D_{\text{co}} = 2.9 \times 10^{-7}$ – $5.5 \times 10^{-7} \text{ cm}^2 \text{ s}^{-1}$, $\alpha_{\text{de}} = 4.7 \text{ cm}^3 \text{ g}^{-1}$ and $D_{\text{col}} = 2.25 \times 10^{-7}$ – $4.5 \cdot 10^{-7} \text{ cm}^2 \text{ s}^{-1}$, $\alpha_{\text{di}} = 12.6 \text{ cm}^3 \text{ g}^{-1}$. Low and high zero-concentration diffusivities corresponds to dry and swollen plate thicknesses, respectively.

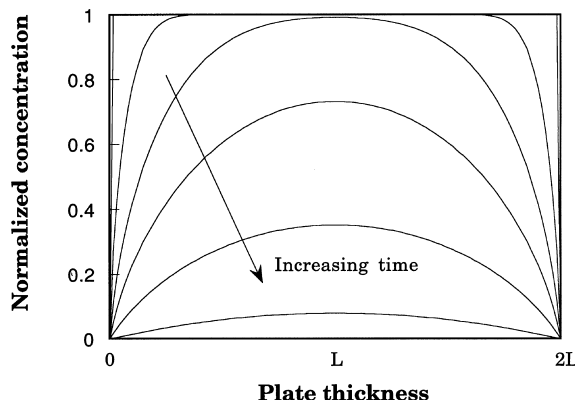


Fig. 6. Concentration profiles generated using Eq. (5) with the parameter values given in Fig. 5.

sorption data of n-hexane–NR were modelled using Eqs. (4) and (5) with very high concentration dependence allowing the diffusivity to vary over several magnitudes (Fig. 7). The numerical multistep formula [Eq. (10)] allows for calculations with very high concentration dependence. As can be seen in Fig. 7, concentration-dependent diffusivity alone does not lead to an s-shaped sorption curve. The concentration profiles associated with a very high concentration-dependent diffusivity become nearly as steep as in case II diffusion (Fig. 8). Case II diffusion is, however, characterized by a mass increase which is proportional to time and not to the square root of time as in this case. Eqs. (4) and (5) yield similar concentration profiles.

When a large amount of a solute enters the polymer matrix, swelling occurs. So far, in the previous treatment, dimensional changes have been neglected except that completely swollen and unswollen sample thicknesses have been used in the diffusion equations. It is expected that, for non-polar systems like n-hexane–NR and n-hexane–LDPE, the volumes of the solute and of the polymer are additive [22]. For the n-hexane–NR system, the saturation

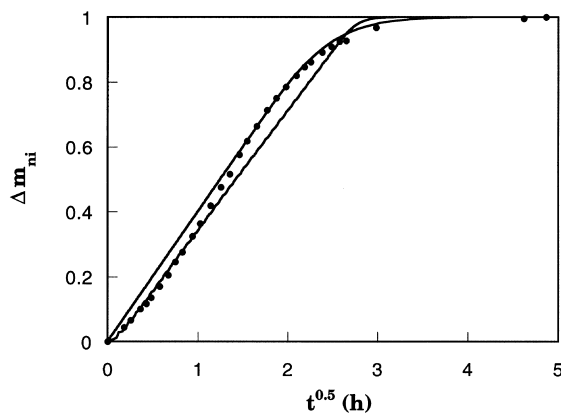


Fig. 7. Eq. (4) [upper line] and Eq. (5) [lower line] applied to sorption data for NR (●). The curves illustrate the effect of using a high concentration-dependence applying the following parameter values: $D_{\text{co}} = 2.10^{-10} \text{ cm}^2 \text{ s}^{-1}$, $\alpha_{\text{De}} = 23.5 \text{ cm}^3 \text{ g}^{-1}$ and $D_{\text{col}} = 8.10^{-19} \text{ cm}^2 \text{ s}^{-1}$, $\alpha_{\text{Di}} = 3.10^{12} \text{ cm}^3 \text{ g}^{-1}$. A dry plate thickness value was used.

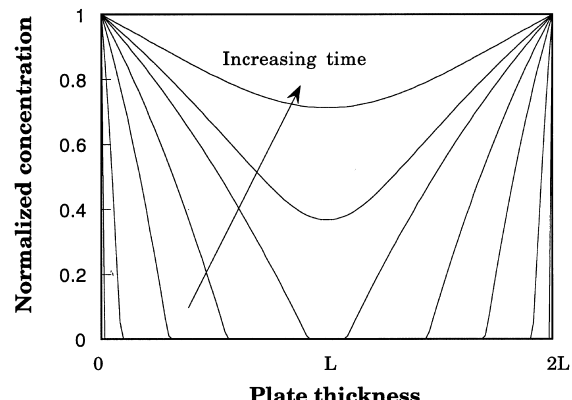


Fig. 8. Concentration profiles obtained from Eq. (5) using the values given in Fig. 7.

n-hexane volume fraction is 0.64 and the calculated volume fraction based on the sample volume increase is 0.65, and for n-hexane–LDPE the corresponding values are 0.13 and 0.11, respectively, which shows that the volumes are almost additive in both systems. Swelling should therefore be proportional to mass uptake, i.e. the sample volume increase with respect to time should have the same curve profile as the mass increase. Figs 9 and 10 show the sample mass and the sample dimensions as a function of the square root of time for NR and LDPE. Evidently the mass and volume increase curves overlap for both NR and LDPE. The increase in cross-sectional area, thickness, mass and volume all follow an s-shape with respect to the square root of time. With regard to the data here reported and also to the data of Mazich et al. [10], it is suggested that the s-shaped sorption (mass increase) in highly swelling systems is due to the fact that, in the initial period, the swelling is mostly one-dimensional (stage I, Fig. 11) because the unswollen core suppresses swelling perpendicular to the main mass flux direction. At later stages, when the core is plasticized by the solute molecules, the sample may swell in all three dimensions. It is evident that the thickness of the LDPE specimen increased more rapidly in the initial stage than the cross-section of the specimen, i.e. the average

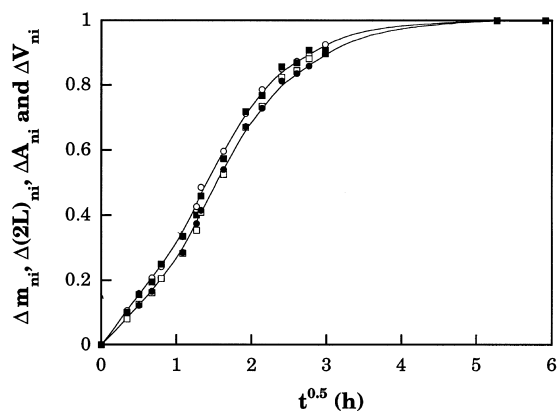


Fig. 9. Normalized mass (●), volume (□), thickness (○) and cross-sectional area (■) increase as a function of time during sorption of n-hexane in NR.

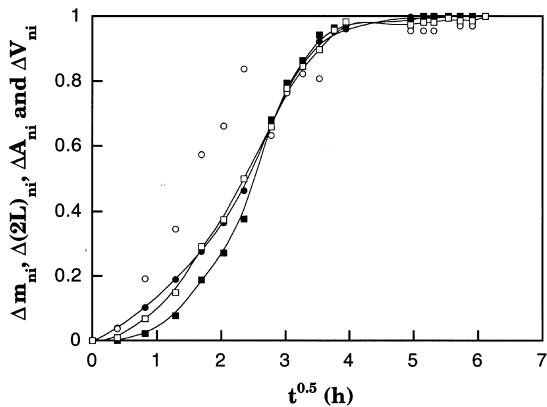


Fig. 10. Normalized mass (●), volume (□), thickness (○) and cross-sectional area (■) increase as a function of time during sorption of n-hexane in LDPE.

normalized thickness-to-cross-sectional area ratio taken over the whole sorption period was high ($tca = 2.45$). For NR the s-shape is less pronounced, and the swelling anisotropy is negligible ($tca = 1.02$). This may be explained by the fact that the bulk modulus, and consequently the ability of the core to withstand the tension exerted by the swollen surface, is less for NR than for LDPE ($K = 2.0$ GPa (NR) and $K = 3.4$ GPa (LDPE) [30], [31]). Interestingly, the bulk modulus ratio between LDPE and NR ($= 1.7$) is of the same order of magnitude as the tca ratio ($= 2.4$). Thus, by determining tca during the transient sorption period, it may be possible to estimate the bulk modulus of the sample if tca is calibrated using a sample of known bulk modulus. The correlation between tca and K obtained here suggests that it is the bulk modulus and not the elastic modulus, as has been suggested by several researchers [20], [21], [26], that determines the ability of a polymer to withstand solute-induced swelling.

Figs 12 and 13 show the sample mass loss and dimensional decrease as a function of desorption time. The curves obtained for NR and LDPE have similar shapes.

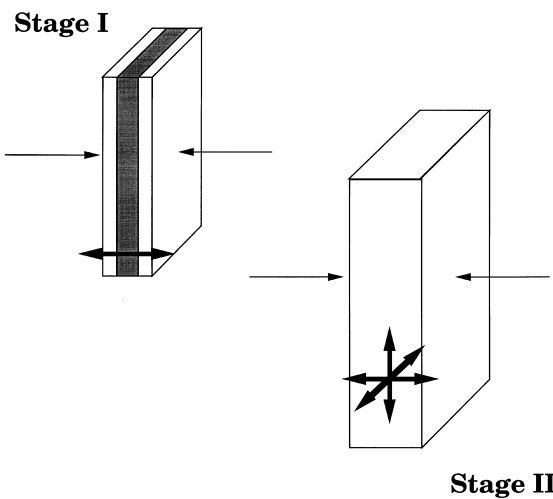


Fig. 11. Model for geometrical changes of specimen during sorption of n-hexane in LDPE. Stage I involves swelling is mainly uni-dimensional swelling whereas at stage II the swelling is three-dimensional.

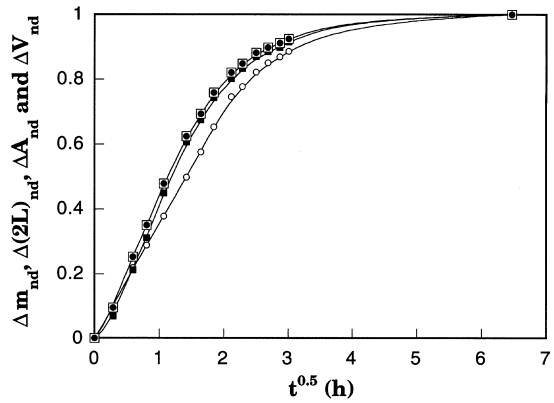


Fig. 12. Normalized mass (●), volume (□), thickness (○) and cross-sectional area (■) decrease as a function of time for desorption of n-hexane.

The cross-sectional area decreased more rapidly than the specimen thickness in both systems. This may be explained by the homogeneous solute concentration distribution during desorption compared to the steep gradients prevailing during sorption. The continuous feed of solute to the surface region from the interior parts leads to a slow decrease in sample thickness. The fact that tca is similar for both LDPE and NR and that the concentration profiles are smooth suggests that mechanical stresses play only a minor role during the transient desorption period.

Using Eqs. (22)–(44) without the stress-terms, the effect of swelling on the sorption curve shape may be analysed. In Fig. 14, the sorption curve for NR is modelled using swelling terms with and without concentration-dependent diffusivities. The swelling itself does not create a significantly s-shaped sorption curve, but, in combination with a large concentration dependence of D , a pronounced s-shape arises. The fitted sorption curve does not resemble the experimental data. Fig. 15 shows the concentration profile using a high concentration dependence and a variable geometry. By modelling, it is further concluded that swelling alone cannot predict the desorption curves unless D is concentration-dependent.

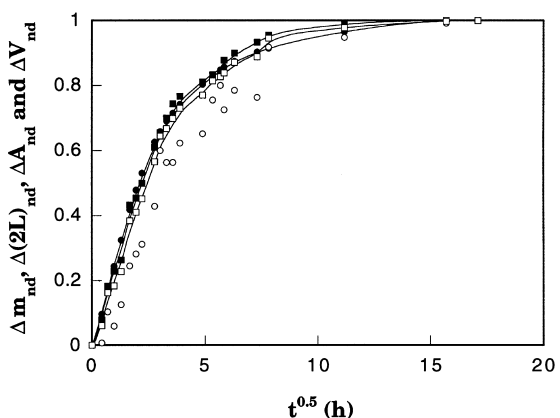


Fig. 13. Normalized mass (●), volume (□), thickness (○) and cross-sectional area (■) decrease as a function of time for desorption of n-hexane from LDPE.

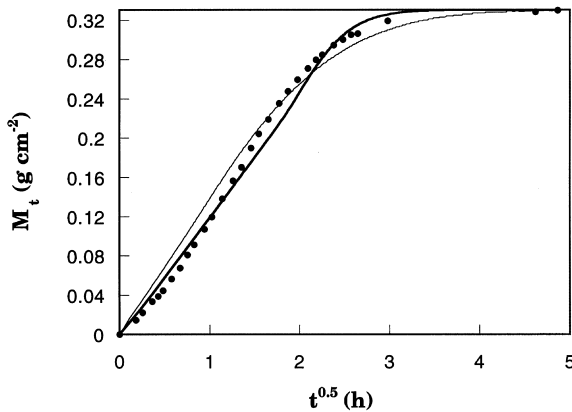


Fig. 14. Eq. (4) including the swelling treatment [Eqs. (22)–(45)] but without stress-terms, applied to data obtained for sorption of n-hexane in NR (•). To simulate a high concentration-dependence, the following values were chosen: $D_{\text{coe}} = 1.3 \times 10^{-8} \text{ cm}^2 \text{ s}^{-1}$, $\alpha_{\text{De}} = 15 \text{ cm}^3 \text{ g}^{-1}$ [thicker curve]. A constant D was introduced using $D_{\text{coe}} = 3.10^{-6} \text{ cm}^2 \text{ s}^{-1}$ and $\alpha_{\text{De}} = 0 \text{ cm}^3 \text{ g}^{-1}$ [thinner curve].

So far, solute-induced mechanical stresses have been considered only qualitatively, but in the following treatment they are included in the calculations. The simplest way to incorporate stress effects is to assume that the surface concentration is time-dependent [Eq. (19)]. Long and Richman [19] reported a time-dependent surface concentration of methyl iodide in cellulose acetate during the transient sorption period. The resulting s-shaped sorption is then primarily determined by the single relaxation time (τ_s) and the initial surface solute concentration C_o . As can be seen in Fig. 16, using $\tau_s = 3 \text{ h}$ and $C_o = 0.49$ (of 1), the fit to the experimental sorption data for NR is perfect. The concentration profiles that generate Fig. 16 are shown in Fig. 17. The corresponding optimum values for LDPE are 104 h and $C_o = 0.7$. For a comparison, the system methanol–glassy poly(ethersulphone) is also perfectly fitted using this simple model, although with a longer relaxation time [$\tau_s = 278 \text{ h}$ and $C_o = 0.7$ (of 1) [13]]. These values were

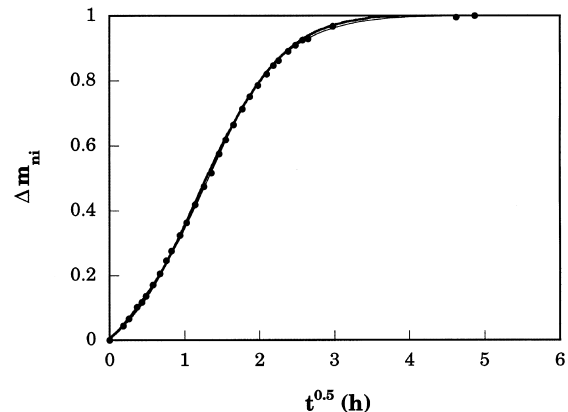


Fig. 16. N-hexane-NR experimental sorption data (•) fitted with Eqs. (4), (6)–(10) and (19); time-dependent boundary concentration, thin line) and with Eqs. (6)–(10) and Eqs. (46)–(50) [layered structure, thick line]. The parameter values obtained by fitting were: $D_{\text{coe}} = 8.5 \times 10^{-7} \text{ cm}^2 \text{ s}^{-1}$, $\alpha_{\text{De}} = 3.1 \text{ cm}^3 \text{ g}^{-1}$ [using dry thickness] and $D_{\text{coe}} = 1.7 \times 10^{-6} \text{ cm}^2 \text{ s}^{-1}$, $\alpha_{\text{De}} = 3.1 \text{ cm}^3 \text{ g}^{-1}$ [swollen thickness]; $\tau = 11236 \text{ s}$ and $C_o = 0.49$; $\xi = 1$, $D_a = 3.2 \times 10^{-7} \text{ cm}^2 \text{ s}^{-1}$ and $D_b = 5 \times 10^{-6} \text{ cm}^2 \text{ s}^{-1}$ [dry thickness].

obtained using the multi-step method [Eq. (10)] and it should be mentioned that the calculated τ_s -values using the Runge–Kutta method were much lower [0.2 h (NR) and 5.6 h (LDPE)]. C_o for NR was calculated to be 0.6 using the Runge–Kutta method. The reason for this discrepancy in relaxation time is not clear. Stress relaxation data on LDPE reported by Becker [32], [33] suggest a stress relaxation time between 6.8 and 20 h, independent of strain level. Nisizawa [34] measured stress decay times of 24–160 h for LDPE immersed in a benzene series of hydrocarbons.

It has been shown theoretically that s-shaped sorption curves may appear in samples with a surface skin with properties different from those of the core [18]. If, for example, the polymer material is surface oxidized, the surface region may have a lower diffusivity than the core. As can be seen in Fig. 16, such a model (Eqs. (46)–(50), layered model) also matches the experimental sorption data perfectly. However, as can be seen in Fig. 18, the layered model cannot fit the desorption data and it has, therefore, not been further considered.

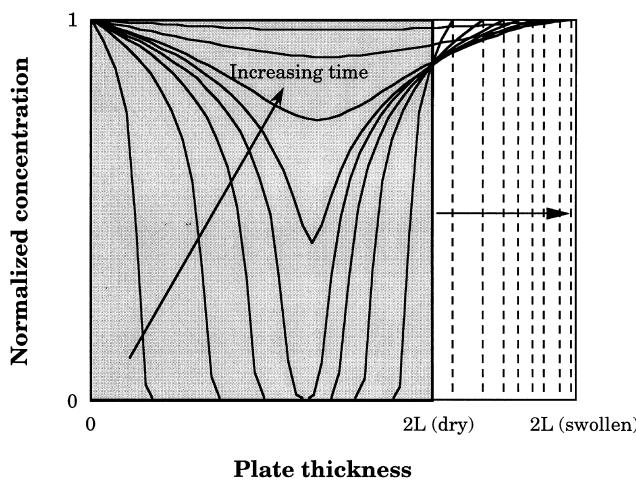


Fig. 15. Concentration profiles generated using Eq. (4) with $D_{\text{coe}} = 1.3 \times 10^{-8} \text{ cm}^2 \text{ s}^{-1}$ and $\alpha_{\text{De}} = 15 \text{ cm}^3 \text{ g}^{-1}$ and including the swelling treatment in Fig. 14.

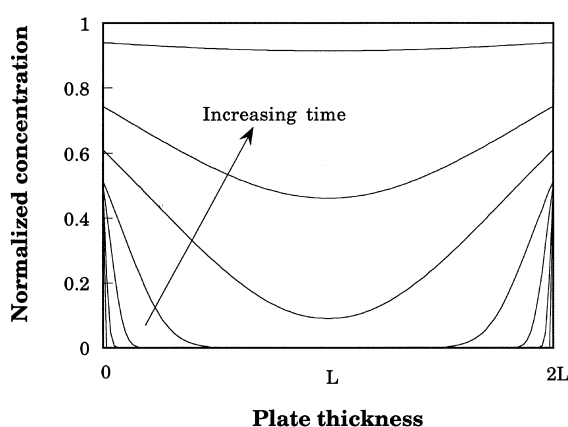


Fig. 17. Concentration profiles generated using Eqs. (4), (6)–(10) and (19) with the parameters used in Fig. 16 (sorption).

An additional, more detailed, stress approach is to use Eqs. (22)–(44). This approach was applied to the sorption data for NR. The parameters D_{coe} , K , τ_m , α_{De} , α_K , and α_{τ_m} were all varied independently in an attempt to obtain an s-shaped sorption curve. In the Maxwell equation, σ_{xx}^s is considered to be zero in all cases for both NR and LDPE. It was shown that, without the use of a concentration-dependent surface concentration, no s-shaped sorption curve was ever obtained. Hence, regardless of what the stress-distribution looks like in the interior of the sample, it is the time-dependent solute concentration at the boundary surface which gives rise to the s-shape. Therefore, in the subsequent treatment, a time-dependent surface concentration was always used. The starting point in the next step in fitting the sorption curves for NR was to use the data obtained earlier ($\tau_s = 0.2$ h and $C_o = 0.6$) and to assume swelling according to Eq. (35). This results in a decrease in D_o from 1×10^{-6} to 6.7×10^{-7} $\text{cm}^2 \text{s}^{-1}$. In the next step, K was introduced without any concentration- or time-dependence. This moved the whole sorption curve to shorter times with only a negligible change in its shape. The effect of introducing K is basically to squeeze solute into the interior of the sample. When K was introduced, D_{coe} decreased from 6.7×10^{-7} to 4.8×10^{-8} $\text{cm}^2 \text{s}^{-1}$ and α_{De} changed from 4.5 to $1.0 \text{ cm}^3 \text{g}^{-1}$. Hence, by introducing a variable sample geometry and a constant bulk modulus, the calculated diffusivity was changed by almost two orders of magnitude. In the next fitting step, stress relaxation was introduced; i.e. τ_m increased from zero to the value of τ_s (0.2 h). This changed the curve shape dramatically and far from the experimental data. No further improvement was achieved by introducing a solute-concentration-dependence ($\alpha_K = \alpha_{\tau_m} = \alpha_{\text{De}} = 1.0 \text{ cm}^3 \text{g}^{-1}$). Thus it was assumed in the subsequent calculations that the parameters α_K and α_{τ_m} were equal to zero. By letting τ_m be small (≈ 0.1 h) (instantaneous stress relaxation) the original

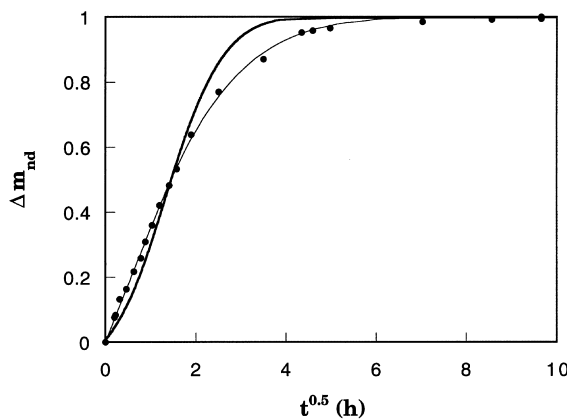


Fig. 18. Experimental desorption data for NR data (●) fitted with Eqs. (3), (4), (6)–(10) [thin line] and with Eqs. (3), (6)–(10) and Eqs. (46)–(50) [thick line]. The parameter values obtained by fitting were: $D_{\text{coe}} = 2.9 \times 10^{-7} \text{ cm}^2 \text{s}^{-1}$, $\alpha_{\text{De}} = 4.7 \text{ cm}^3 \text{g}^{-1}$ [using dry thickness] and $D_{\text{coe}} = 5.5 \times 10^{-7} \text{ cm}^2 \text{s}^{-1}$, $\alpha_{\text{De}} = 4.7 \text{ cm}^3 \text{g}^{-1}$ [swollen thickness] and $F_o = 3 \times 10^{-5} \text{ cm s}^{-1}$; $\xi = 1$, $D_a = 3.2 \times 10^{-7} \text{ cm}^2 \text{s}^{-1}$ and $D_b = 5 \times 10^{-6} \text{ cm}^2 \text{s}^{-1}$ [dry thickness].

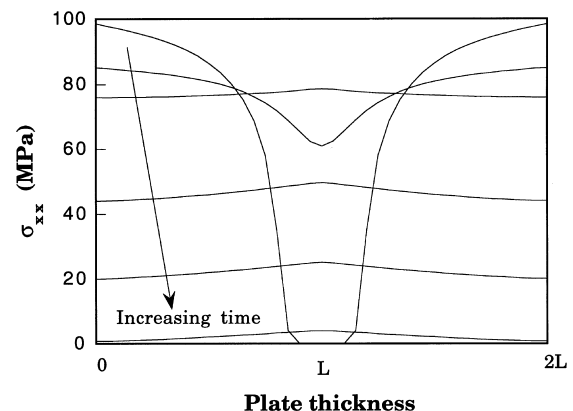


Fig. 19. Solute-induced mechanical stress profiles as a function of time for the sorption of n-hexane in LDPE using Eqs. (4), (22)–(45) with parameters the same as those in Table 1, except that $K_{\text{co}} = 3.4 \text{ GPa}$ and $\tau_{\text{mco}} = 5.6 \text{ h}$.

curve, i.e. with $K = 0$, was obtained. No further modelling using other values for τ_m , α_K and α_{τ_m} was performed, since it is believed that no further improvement could be achieved by varying these parameters. It should be mentioned that the surface concentration is considered in the present study not to be solute-concentration-dependent ($\alpha_{\tau_s} = 0 \text{ m}^3 \text{kg}^{-1}$) since the fitting is sufficiently good with a constant τ_s . Fig. 19 shows an example of stress distributions in a specimen. The modelling of sorption in NR given in Table 1 suffices to describe both the mass increase and the dimensional (thickness) increase during sorption (Fig. 20). Table 1 presents the parameters used to fit the sorption data of LDPE. As can be seen in Fig. 21, the model fails to predict the thickness increase of LDPE unless the swelling parameter (*sp*) is increased from 1/3 to 1/1.7 during stage I. This suggests a higher anisotropy of swelling during the transient sorption period in LDPE than in NR.

Even though systems exhibiting Case-II diffusion may show s-shaped sorption curves, there is a clear difference between these and the systems reported here. For systems showing Case-II diffusion the sorption curves of samples having different thicknesses do not collapse into one single

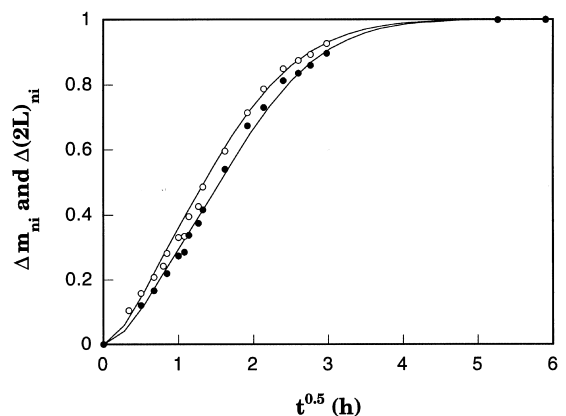


Fig. 20. Experimental sorption data for NR (●) and thickness increase (○) fitted with Eqs. (4), (22)–(45) using the parameter values given in Table 1. The continuous lines are best fits.

Table 1
Parameters used for fitting NR and LDPE sorption–desorption data

| Parameter | NR Sorption | NR Desorption | LDPE Sorption | LDPE Desorption |
|--|----------------------|-----------------------|------------------------|----------------------|
| $D_{\text{co}} (\text{cm}^2 \text{s}^{-1})$ | 6.7×10^{-7} | 4.05×10^{-7} | 2.5×10^{-9} | 1.4×10^{-8} |
| $\alpha_{\text{De}} (\text{cm}^3 \text{g}^{-1})$ | 4.5 | 8.05 | 70 | 52 |
| $\tau_{\text{mc}} (\text{h})$ | — | — | — | — |
| $\alpha_{\text{rm}} (\text{cm}^3 \text{g}^{-1})$ | — | — | — | — |
| $K_{\text{co}} (\text{MPa})$ | — | — | — | — |
| $\alpha_{\text{K}} (\text{cm}^3 \text{g}^{-1})$ | — | — | — | — |
| C_o | 0.6 | — | 0.7 | — |
| $\tau_{\text{sco}} (\text{h})$ | 0.2 | — | 5.6 | — |
| $\alpha_{\text{rs}} (\text{cm}^3 \text{g}^{-1})$ | — | — | — | — |
| sp | 0.33 | 0.33 | 0.59–0.33 ^a | > 0.33 |
| $M_1 (\infty) (\text{kg m}^{-2})$ | 3.74 | 3.74 | 0.19–0.197 | 0.19–0.197 |

^ainitially 0.59 and at later stages 0.33

curve when the normalized mass is plotted as a function of time normalized with sample thickness[6]. Data presented here ‘collapse’ into a single curve and hence the thickness does not seem to be a parameter affecting the diffusivity and relaxation properties of the present systems (Fig. 22).

Fig. 23 presents the fit of desorption data of NR using a variable geometry. The use of a variable geometry in the modelling increased the diffusivity from $2.7 \times 10^{-7} \text{ cm}^2 \text{s}^{-1}$ (using a constant swollen thickness) to $4.05 \times 10^{-7} \text{ cm}^2 \text{s}^{-1}$ whereas the curve shape was essentially unchanged (α_{De} changed from 8.5 to $8.05 \text{ m}^3 \text{kg}^{-1}$). These values are similar to the data obtained by fitting the desorption data of NR using the multi-step formula given by Eq. (10), (Fig. 5). The use of $sp = 1/3$ over the whole desorption period seems also to predict the thickness variation, although a small deviation was noticed which suggests that a small anisotropy in shrinking occurred during the initial stage of desorption. For LDPE, however, the model was unable to fit the thickness decrease (Fig. 24). This is probably because, in the initial stage, sp is larger than 1/3

whereas at later stages the sample shrinks isotropically ($sp = 1/3$). This may be observed by looking at the rate of thickness decrease which shows an s-shape in the early stage and a curve shape similar to that of the mass decrease at longer times. As in the case of sorption, the introduction of K , τ_{m} , α_{K} and $\alpha_{\tau_{\text{m}}}$ in the modelling of the desorption data provided no contribution to the fitting of the mass and thickness decrease and these parameters were, therefore, omitted.

When sorption and desorption data are compared, time effects, e.g. non-reversible material changes occurring due to the course of time, may become important. These effects are more prominent in LDPE than in NR; (cf. D_{co} -values obtained from sorption and desorption data in Table 1). For NR these values are similar, but for LDPE the values obtained from desorption data are larger than for those obtained from sorption data. Hedenqvist et al. [2] suggested that the penetrant caused a loosening of constrained tie chains.

Finally, knowing what parameters primarily affect the sorption–desorption curves (Table 1), a general description of the curves for highly swollen polymers above T_g is given in Fig. 25. The general placement of the sorption curve on the $t^{0.5}$ -scale is determined mainly by the D_{co} , α_{De} , C_o and t_s

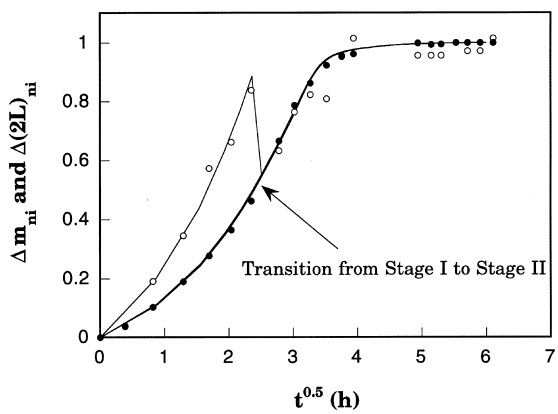


Fig. 21. Experimental sorption data for LDPE (●) and thickness increase (○) — fitted with Eqs. (4), (22)–(45) using the parameter values given in Table 1. The fitted curve for the thickness increase using $sp = 0.33$ over the entire sorption period coincides precisely with the fitted curve for the mass increase. The continuous thin line fitted to the thickness increase data is obtained by using $sp = 0.59$ initially (stage I) and $sp = 0.33$ at later times (stage II).

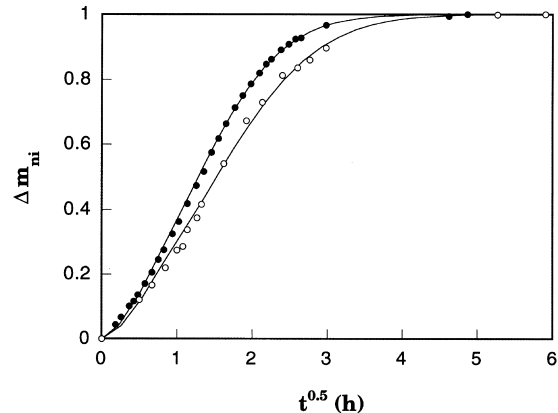


Fig. 22. Experimental sorption data for NR using samples of different thicknesses — (●) $2L = 2.715 \text{ cm}$; (○) $2L = 3.26 \text{ cm}$ — fitted with Eqs. (4), (22)–(45) using the parameter values given in Table 1. The continuous lines are best fits.

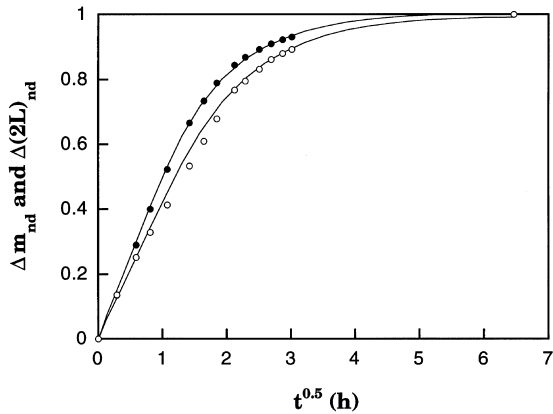


Fig. 23. Experimental desorption data for NR — samples mass (●) and thickness decrease (○) fitted with Eqs. (4), (22)–(45) using the parameter values given in Table 1. The continuous lines are best fits.

values, whereas the curve-shape (s-shape) at the initial stages of sorption is determined only by C_o and t_s . If the concentration-dependence is high (α_{De} is high) the sorption fronts become steep and therefore, when they meet in the final stages of sorption, there will be an abrupt change in the sorption curve. The curvature at the end of sorption is determined by α_{De} and, if the boundary concentration is time-dependent, the time to complete saturation is determined by t_s . Desorption involves less parameters and the overall position of the desorption curve on the $t^{0.5}$ -scale is primarily given by D_{coe} and α_{De} . If the desorption process is evaporation-controlled rather than diffusion-controlled, the desorption curve will be s-shaped. The curvature will then be determined by the evaporation constant F_o . Except for the s-shape, which is often absent, the curve-shape will be determined only by α_{De} .

6. Conclusions

The direct use of mechanical stresses and mechanical relaxation parameters in the present modelling gave little

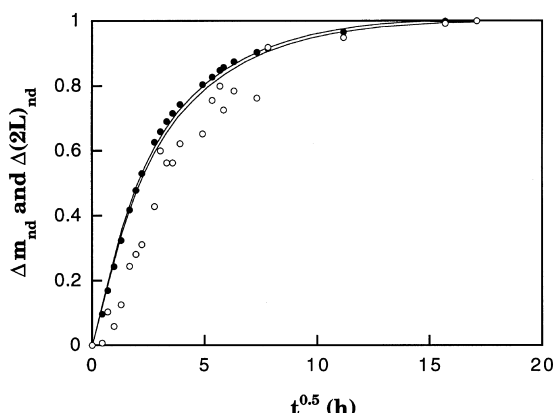


Fig. 24. Experimental desorption data for LDPE — samples mass (●) and thickness decrease (○) fitted with Eqs. (4), (22)–(45) using the parameter values given in Table 1. The continuous lines (upper, mass; lower, thickness) are best fits.

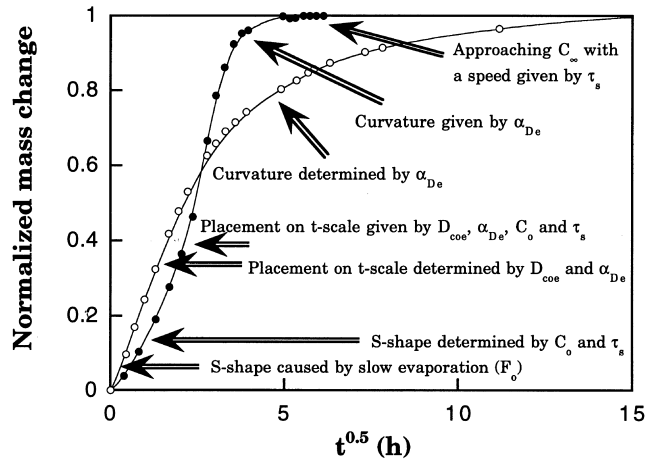


Fig. 25. Parameters determining the shape of n-hexane—LDPE sorption and desorption curves; (●) sorption and (○) desorption.

or no improvement of the fit to experimental sorption and desorption data. The indirect use of stresses via a time-dependent surface concentration was successful in fitting the s-shaped sorption curves obtained for both natural rubber and low-density polyethylene. This method could also describe the thickness variations in samples of natural rubber during both the transient sorption and desorption periods. For low-density polyethylene, on the other hand, a model consisting of two different stages had to be adopted. In stage I, the swelling was mainly uni-dimensional along the thickness direction. Stage II, occurring at later times, was characterized by fully three-dimensional swelling. During the transient sorption period, the ratio of the thickness-to-cross-sectional-area ratio between natural rubber and low-density polyethylene was of the same order of magnitude as their bulk modulus ratio, which suggests that it is the bulk modulus rather than the Young's modulus which determines the sorption characteristics of polymers above the glass transition temperature.

Acknowledgements

The Sweden-American Foundation and the Swedish Institute are gratefully acknowledged for making this work possible. Professor Josef Kubat, Department of Polymeric Materials, Chalmers University of Technology and Dr. Sören Östlund, Department of Solid Mechanics, Royal Institute of Technology are thanked for fruitful discussions.

References

- [1] Hedenqvist M, Varkalis A, Johnsson G, Gedde UW. *Thermochim Acta* 1993;214:111.
- [2] Hedenqvist M, Tränkner T, Johnsson G, Gedde UW. *Polym Engng Sci* 1995;36:4359.
- [3] Crank J. *The mathematics of diffusion*, 2nd ed. Oxford: Clarendon Press, 1986.

- [4] Crank J. In: Comyn J, editor. *Polymer permeability*, 2nd ed. Oxford: Clarendon Press, 1986.
- [5] Crank J, Park GS. *Diffusion in polymers*. New York: Academic Press, 1968.
- [6] Neogi P. In: Neogi P, editor. *Diffusion in polymers*. New York: Marcel Dekker, 1996.
- [7] Neogi P. *J Polym Sci, Polym Phys Edn* 1993;31:699.
- [8] Browne MM, Forsyth M, Goodwyn AA. *Polymer* 1995;36:4359.
- [9] Rossi G. *Trends Polym Sci* 1996;4:337.
- [10] Mazich KA, Rossi G, Smith CA. *Macromolecules* 1992;25:6929.
- [11] Samus MA, Rossi G. *Macromolecules* 1996;29:2275.
- [12] Billovits GF, Durning CJ. *Polymer* 1988;29:1468.
- [13] Wiberg G, Hedenqvist M, Gedde UW. *Polym Engng Sci*, in press.
- [14] Neogi P, Kim M, Yang Y. *AIChE J* 1986;32:1146.
- [15] Crank J. *J Polym Sci* 1953;11:151.
- [16] Nath SK. *Comp Polym Sci* 1995;5:171.
- [17] Waksman LS, Schneider NS, Sung N-H. In: Koros WJ, editor. *Barrier polymers and structures*. ACS Symposium Series No. 423. Washington, DC: American Chemical Society, 1990.
- [18] Crank J, Park GS. *Trans Faraday Soc* 1951;47:1072.
- [19] Long FA, Richman D. *J Am Chem Soc* 1960;82:513.
- [20] Neogi P. *AIChE J* 1983;29:829.
- [21] Doghieri F, Roda GC, Sarti GC. *AIChE J* 1993;39:1847.
- [22] Hedenqvist M, Angelstok A, Edsberg L, Larsson PT, Gedde UW. *Polymer* 1996;37:2887.
- [23] Bakhouya A, El Brouzi A, Bouzon J, Vergnaud JM. *Plast Rubber Comp Proc Appl* 1993;19:77.
- [24] Hedenqvist M, Ohrlander M, Palmgren R, Albertsson A-C. *Polym Engng Sci*, in press.
- [25] Kahaner D, Moler C, Nash S. *Numerical methods and software*. Englewood Cliffs, NJ: Prentice-Hall, 1989.
- [26] Wu JC, Peppas NA. *J Polym Sci, Polym Phys Ed* 1993;31:1503.
- [27] Fung YC. *Foundations of solid mechanics*. Englewood Cliffs, NJ: Prentice-Hall, 1965.
- [28] Street RL, Watters GZ, Vennard JK. *Elementary fluid mechanics*, 7th ed. New York: Wiley, 1996.
- [29] Fujita H. *Fortschr Hochpol Forsch* 1961;3:1.
- [30] van Krevelen DW. *Properties of polymers*, 2nd ed. Amsterdam: Elsevier, 1976.
- [31] Tabor D. *Polymer* 1994;35:2759.
- [32] Becker GW. *Kolloid Z* 1961;175:99.
- [33] Becker GW, Rademacher H-J. *J Polym Sci* 1962;58:621.
- [34] Nisisawa M. *J Appl Polym Sci* 1969;13:1621.